

Optical Properties of Perovskite Oxides in Their Paraelectric and Ferroelectric Phases

M. DiDOMENICO, JR., AND S. H. WEMPLE

Bell Telephone Laboratories, Murray Hill, New Jersey

(Received 31 May 1967; revised manuscript received 13 September 1967)

The optical-absorption characteristics of the perovskite oxides BaTiO₃, KTaO₃, and KTa_{0.65}Nb_{0.35}O₃ (KTN) are reported in the vicinity of the interband absorption edge, and, in the case of semiconducting KTN, in the near infrared where donor photo-ionization absorption dominates. The large optical-absorption anisotropies observed in the ferroelectric phases of BaTiO₃ and KTN are shown to be related to shifts in conduction-band valleys by using a many-valley model with three valley minima at the zone boundary along the (100) directions. The two valleys lying along axes perpendicular to the direction of the spontaneous polarization P_s are raised in energy by an amount $\Delta\epsilon \propto P_s^2$ relative to the valley parallel to P_s , where $\Delta\epsilon = 2.2P_s^2$ eV for KTN and $\Delta\epsilon = 1.5P_s^2$ eV for BaTiO₃ (P_s is in C/m²). In the case of KTN the valley energy shifts are found to be consistent with electrical-conductivity anisotropy data. The interband-absorption-edge data are found to show an exponential Urbach tail in all three materials up to absorption coefficients of at least 10⁹ cm⁻¹. The band-edge results for BaTiO₃ are in disagreement with existing published data. The donor photo-ionization data in semiconducting KTN and the attendant large dichroism are shown to be governed by a simple f sum rule.

1. INTRODUCTION

THE ABO_3 perovskite oxides have been of continuing interest because of their ferroelectric and electro-optic properties. Recently, interest has been directed at the energy-band structure of these materials in an effort to understand the results of a wide variety of experiments, including ultraviolet reflectivity,^{1,2} electroreflectivity^{2,3} and electroabsorption,⁴ electrical conductivity and Hall effect,^{5,6} magnetoresistance,⁷ piezoresistance,^{8,9} cyclotron resonance,¹⁰ and superconductivity.¹¹ In the present work we report on the optical-absorption characteristics of three members of the ABO_3 family, viz., insulating BaTiO₃, insulating KTaO₃, and both insulating and semiconducting KTa_{0.65}Nb_{0.35}O₃ (KTN). The principal aims are to relate the optical properties to the energy-band structure and to the electrical conductivity, and to show how the ferroelectric phase transition affects the optical properties via its effect on the energy bands.

2. BAND STRUCTURE AND TRANSPORT PROPERTIES

Theoretical predictions of the energy-band structure of the perovskite oxides, in particular SrTiO₃, have been made by Kahn and Leyendecker¹² (KL). Their linear combination of atomic orbitals (LCAO) or tight-binding results suggest that the conduction band is many-valleyed with equivalent minima along $\langle 100 \rangle$ directions at the Brillouin zone boundary. The magnetore-

sistance data^{7,13} in SrTiO₃ and KTaO₃, particularly the very high field measurements in SrTiO₃, appear to substantiate the conclusion of zone boundary minima, although this conclusion is not totally unambiguous since it may be possible for suitably warped spheres at the zone center ($k=0$) to give the same result. Lacking any absolute evidence for a $k=0$ minimum, we have based our data analysis on a many-valley model with the point of view of looking for internal inconsistencies. Berglund and Baer,¹⁴ in their analysis of BaTiO₃ conductivity data, have taken a similar viewpoint.

According to KL the valence band in the perovskite oxides is primarily an oxygen $2p$ band, whereas the lowest conduction band is derived from the transition-metal B -cation $d\epsilon$ d orbitals. The tight-binding electronic energy-band structure of KL for SrTiO₃ is partially shown in Fig. 1(a) for the $d\epsilon$ conduction band and the upper valence bands. Because the $(p\bar{p}\pi)$ and $(p\bar{p}\sigma)$ interactions are small, the top of the valence band is relatively flat or very nearly a pure atomic \bar{p} state. In the lowest conduction band, the large band bending X_3-M_5 along Z_4 arises from a large $(p\bar{d}\pi)$ overlap, giving rise to a reasonably small transverse effective mass. The longitudinal mass, on the other hand, is thought to be large because the band bending $\Gamma_{25'}-X_3$ along Δ_2'

⁷ H. P. R. Frederikse, W. R. Hosler, and W. R. Thurber, Phys. Rev. **143**, 648 (1966); H. P. R. Frederikse, W. R. Hosler, W. R. Thurber, J. Babiskin, and P. G. Siebenmann, *ibid.* **158**, 775 (1967).

⁸ O. N. Tufte and E. L. Stelzer, Phys. Rev. **141**, 675 (1966).
⁹ S. H. Wemple, A. Jayaraman, and M. DiDomenico, Jr., Phys. Rev. Letters **17**, 142 (1966).

¹⁰ L. S. Senhouse, G. E. Smith, and M. V. DePaolis, Phys. Rev. Letters **15**, 776 (1965).

¹¹ See, for example, J. F. Schooley, W. R. Hosler, and M. L. Cohen, Phys. Rev. Letters **12**, 474 (1964); J. F. Schooley, W. R. Hosler, E. Ambler, J. H. Becker, M. L. Cohen, and C. S. Koonce, *ibid.* **14**, 305 (1965).

¹² A. H. Kahn and A. J. Leyendecker, Phys. Rev. **135**, A1321 (1964).

¹³ I. Camlibel (unpublished).

¹⁴ C. N. Berglund and W. S. Baer, Phys. Rev. **157**, 358 (1967).

¹ M. Cardona, Phys. Rev. **140**, A651 (1965).

² S. K. Kurtz, in *Proceedings of the International Meeting on Ferroelectricity*, edited by V. Dvorak, A. Fouskova, and P. Glogar (Publishing House, Czechoslovak Academy of Sciences, Prague, Czechoslovakia, 1966), Vol. 1, p. 413; also, S. K. Kurtz, T. C. Rich, and W. J. Cole (to be published).

³ A. Frova and P. J. Boddy, Phys. Rev. Letters **16**, 688 (1966).

⁴ A. Frova and P. J. Boddy, Phys. Rev. **153**, 606 (1967).

⁵ H. P. R. Frederikse, W. R. Thurber, and W. R. Hosler, Phys. Rev. **134**, A442 (1964).

⁶ S. H. Wemple, Phys. Rev. **137**, A1575 (1965).

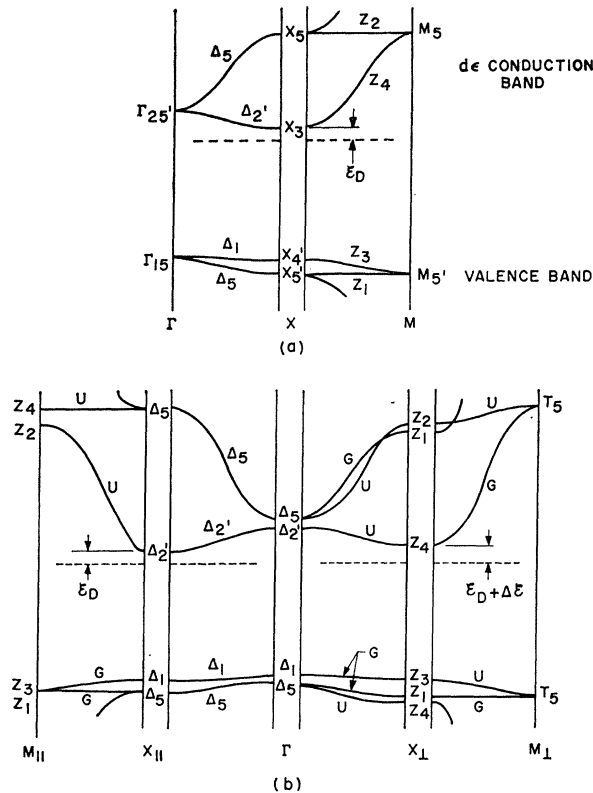


FIG. 1. (a) Kahn and Leyendecker (Ref. 12) tight-binding energy-band structure for the upper valence bands and lowest $d\epsilon$ conduction band for the ABO_3 perovskite oxides. (b) Brews' (Ref. 15) modified band scheme for tetragonally distorted (ferroelectric) perovskite oxides. A deep donor level connected with the X_3 conduction band minimum is indicated schematically by a dashed line in both (a) and (b).

determined largely by the small (ddd) overlap of the B cations over the full $\approx 4\text{-}\text{\AA}$ lattice spacing. According to KL this small band bending places the conduction band minima along $\langle 100 \rangle$ directions at the Brillouin zone boundary. Since the (ddd) interaction is small, the $\Gamma_{25'}-X_3$ tight-binding state is almost a pure atomic d state.

At the Curie point, the crystal symmetry of the ferroelectric perovskites (e.g., KTN and BaTiO_3) is lowered from O_h to C_{4v} . Optical-absorption anisotropies (dichroism) are therefore expected in both band-to-band and donor photo-ionization absorption. In relating the dichroism to the KL many-valley model and the crystal spontaneous polarization, we have made use of recent calculations of Brews¹⁵ and Casella¹⁶ which estimate the distortions in the band structure introduced by the crystal polarization.

In Fig. 1(b) we show the modified energy-band structure, below the cubic to tetragonal ferroelectric transition, brought about by the displacement of the transition-metal ion from the center of the oxygen octa-

hedron toward one of the oxygen ions along a crystalline axis. The band structure of Fig. 1(b) summarizes in part the results of an analysis performed by Brews¹⁵ of the polarization dependence of the LCAO band scheme for SrTiO_3 . As can be seen from the left-hand portion of Fig. 1(b), the tight-binding states in the direction parallel to the lattice polarization (subscript \parallel) are largely unaffected by the tetragonal distortion of the unit cell, except for the splitting at the Γ_{25} point and the splitting at the M_5 point due to the raising of the flat Z_2 level. In the direction perpendicular to the polarization (subscript \perp) there are further splittings and shiftings of the levels as shown in the right-hand portion of Fig. 1(b). Perhaps the most important of these for our purposes is the movement of the upper Z_4 point at X_{\perp} to higher energies. This suggests that in the tetragonal ferroelectric phase the two a -axis valleys lying perpendicular to the direction of spontaneous polarization move up in energy relative to the c -axis valley lying parallel to the polarization direction. The top of the valence band is not strongly affected by the spontaneous polarization because the ($pp\pi$) and ($pp\sigma$) overlaps are small. Furthermore, the calculations also indicate that the ellipsoidal energy surfaces at X_3 are not significantly distorted in the ferroelectric phase. We have therefore based our data analysis on a simple energy shift of equivalent valleys when the crystal becomes ferroelectric. We shall relate the magnitude of this energy shift to the spontaneous polarization and also to the electrical-conductivity anisotropy associated with electron repopulation among the valleys.

For the many-valley model shown in Fig. 1 we can estimate the band bendings $\Delta\epsilon$ along Δ_2' and Z_4 using a simple tight-binding interpolation between zone boundary points of the form $\epsilon(k) = (\Delta\epsilon/2)(1 \pm \cos ka)$, where a is the lattice constant. It can then be shown that

$$\Delta\epsilon \approx m_0/m^* eV, \quad (1)$$

where m_0 is the free-electron mass, and m^* is the effective mass along either the transverse or longitudinal mass directions. The mass data, calculated band bendings, and other pertinent data are shown in Table I for a number of perovskite oxides. Masses have been taken from thermoelectric power,^{5,7,13} Faraday rotation,¹⁷ magnetoresistance,^{7,12} and magnetic-susceptibility data.¹⁸ It is worth noting that d bands in perovskite oxides are not particularly narrow when compared with more conventional semiconductors. Their very low mobility stems from the short relaxation time, in the vicinity of 10^{-14} sec at room temperature. The consequent energy uncertainty is ~ 0.1 eV; this exceeds the room-temperature thermal energy $kT \approx 0.026$ eV, suggesting that the usual electron-scattering theories may not apply to these materials. From hydrostatic piezoresistance measure-

¹⁷ W. S. Baer, Phys. Rev. Letters **16**, 729 (1966); J. Phys. Chem. Solids **28**, 677 (1967).

¹⁸ H. P. R. Frederikse and G. A. Candela, Phys. Rev. **147**, 583 (1966).

¹⁵ J. R. Brews, Phys. Rev. Letters **18**, 662 (1967).

¹⁶ R. C. Casella, Phys. Rev. **154**, 743 (1967).

TABLE I. Some properties of *d*-band perovskite oxides.

Material	Electron Hall mobility at 295°K (cm ² /V sec)	Band gap (see text) (eV)	Estimated $\Delta\epsilon_t = \epsilon_{25} - X_3$ (eV)	Estimated $\Delta\epsilon_t = X_5 - X_3$ (eV)	T_c	P_0 (C/m ²)
SrTiO ₃	5 ^a	3.4 ^b	0.1–0.2	1	32°K ^c	...
BaTiO ₃	≈ 1 ^d	3.3	0.1	1	133°C	0.18 ^e
KTN	3 ^f	3.6	0.3	2	10°C	0.086
KTaO ₃	30 ^g	3.9	1	3	4°K ^h	...

^a See Ref. 5.^b L. Grabner, M. I. Cohen, and R. F. Blunt, *Bull. Am. Phys. Soc.* **11**, 86 (1966).^c G. A. Samara and A. A. Giardini, *Phys. Rev.* **140**, A954 (1965).^d See Ref. 14.^e F. Jona and G. Shirane, *Ferroelectric Crystals* (The Macmillan Company, New York, 1962).^f See Ref. 22.^g See Ref. 6.

ments we have concluded that the primary electron scatterer is the transverse optical "soft mode" associated with the ferroelectricity.^{9,19}

Associated with the X_3 conduction-band minimum in Fig. 1 we show a donor level extending over most of the Brillouin zone. These donors, thought to be oxygen vacancies, can be introduced into KTN by proper adjustment of crystal-growth conditions.^{20,21} Conductivity studies²² have shown this level to be relatively deep (≈ 0.3 eV), leading to a spreading of the level throughout a large fraction of the zone. Donor photoionization absorption from this level to the conduction-band states will be discussed in detail in the following sections.

3. EXPERIMENTAL

A. Absorption Data

The optical-absorption characteristics of extrinsic *n*-type crystals of KTN and insulating crystals of

TABLE II. Room-temperature single-term Sellmeier dispersion parameters for the refractive index in the expression $n^2 - 1 = S/[1 - (\lambda_s/\lambda)^2]$.

Material	S	λ_s (m μ)
KTN ^a	3.80	201
KTaO ₃ ^b	3.66	191
BaTiO ₃ ^c	$S_{\parallel} \approx 3.92$ $S_{\perp} = 4.16$	$\lambda_{\parallel} \approx 211$ $\lambda_{\perp} \approx 216$

^a See Ref. 32.^b V. L. Rideout and S. H. Wemple, *J. Opt. Soc. Am.* **56**, 749 (1966).^c Values given were extracted from data of M. S. Shumate, *Appl. Phys. Letters* **5**, 178 (1964). The subscripts \parallel and \perp denote the light polarization directions relative to the lattice polarization direction.

¹⁹ The transport properties of several perovskite oxides will be reported in detail in a subsequent paper.

²⁰ W. A. Bonner, E. F. Dearborn, and L. G. Van Uitert, in *Crystal Growth*, edited by H. S. Peiser (Pergamon Press, Inc., New York, 1967), p. 437.

²¹ Donors can also be introduced into BaTiO₃ crystals by reduction in hydrogen. For the optical properties of reduced BaTiO₃ see C. N. Berglund and H. J. Braun, *Phys. Rev.* (to be published).

²² S. H. Wemple and S. K. Kurtz, *Bull. Am. Phys. Soc.* **11**, 401 (1966).

KTN, BaTiO₃, and KTaO₃ were measured between 0.1 and 3.5 eV. The KTN crystals had free-electron concentrations in the range of 10¹⁷ to 10¹⁸ cm⁻³ and donor densities in the neighborhood of 10¹⁹ cm⁻³.²³ In all cases the crystals were mechanically polished with a 6- μ diamond paste on a flat tin lap.

Most of the absorption measurements were made with a Beckman Model DK-1A spectrophotometer. This instrument was equipped with a pair of Glan-Thompson polarizing prisms and a sample holder which could be cooled thermoelectrically or heated. Data were taken from photon energies of about 0.4 to about 3.5 eV with a resolution of 10 meV at ≈ 0.4 eV and 5 meV at ≈ 3 eV. The insulating crystals of KTN, BaTiO₃, and KTaO₃ were investigated only in the region of the band edge since these crystals are essentially transparent from ≈ 0.1 eV to the band edge. To extend the absorption data down to photon energies of 0.1 eV in semiconducting KTN, relative absorption measurements were taken with a Beckman Model IR-7 spectrophotometer.

Since the semiconducting KTN crystals transformed to single-domain crystals below their Curie point owing to the elimination of depolarizing fields by the free electrons,²⁴ absorption measurements could be made with polarized light in the ferroelectric phase. Thus, the temperature dependence of the band-edge absorption and the donor photoionization absorption could be measured for light polarized parallel to and perpendicular to the *c* axis of the crystal. The temperature dependence of the dc conductivity was also measured in order to relate the lattice-polarization-induced conduction-band valley splittings to electron repopulation among these valleys below the Curie point.

All of the absorption data reported in this paper were corrected for surface reflections over the full spectral range using the following relation derived from the

²³ S. H. Wemple, D. Kahng, C. N. Berglund, and L. G. Van Uitert, *J. Appl. Phys.* **38**, 799 (1967).

²⁴ M. DiDomenico, Jr., and S. H. Wemple, *Phys. Rev.* **155**, 539 (1967).

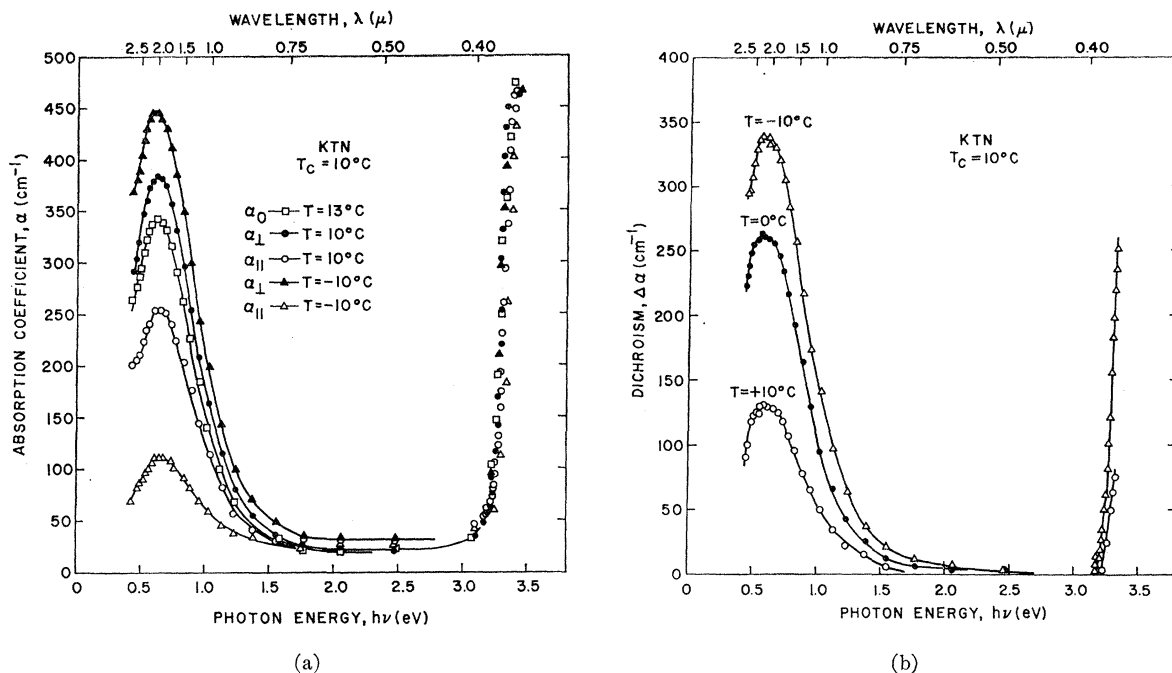


FIG. 2. Spectral dependence of the optical absorption in semiconducting KTN having a free-electron concentration of $3 \times 10^{17} \text{ cm}^{-3}$. (a) Absorption coefficient α versus photon energy $h\nu$ at various temperatures, and (b) dichroism $\Delta\alpha$ versus $h\nu$ at several temperatures below the Curie point.

well-known multiple reflection formula²⁵

$$\alpha \approx \alpha_m - (2R/l) [1 + \frac{1}{2}R(1-t^2)], \quad (2)$$

in which α is the true absorption coefficient, α_m is the measured absorption coefficient, R is the surface reflectivity calculated from refractive index data, t is the measured transmission ratio, and l is the sample thickness. The surface reflectivity $R = (n-1)^2/(n+1)^2$ was calculated using the Sellmeier dispersion relation for the index of refraction n :

$$n^2 - 1 = S/[1 - (\lambda_s/\lambda)^2], \quad (3)$$

where S and λ_s are given in Table II. In the ferroelectric phases of KTN and BaTiO_3 , the small birefringence and temperature dependence of n have been neglected in the calculation of R .

The absorption coefficient α as a function of photon energy $h\nu$ for a KTN crystal having a free carrier concentration of $3 \times 10^{17} \text{ cm}^{-3}$ is shown in Fig. 2(a) at various temperatures above and below the Curie temperature of $T_c = 10^\circ\text{C}$. In the ferroelectric phase, curves of $\alpha_{||}$ and α_{\perp} versus $h\nu$ are given where the subscripts $||$ and \perp refer, respectively, to light polarized parallel to and perpendicular to the direction of spontaneous polarization. Figure 2(b) shows the variation of $\Delta\alpha = \alpha_{\perp} - \alpha_{||}$ with $h\nu$ at several temperatures below T_c . A number of features of the absorption data are of in-

terest. The first is that the band edge obeys Urbach's rule; this will be made clear below. The second is the broad infrared donor photo-ionization absorption band peaking at 0.62 eV. The dichroism $\Delta\alpha$ observed at the absorption peak at the lowest measured temperature of -10°C is very large. We note also that in the visible region just below the band edge, the absorption is larger for $T < T_c$ than for $T > T_c$ for both polarizations of light. Very little dichroism was observed in this region at any temperature.

The band-edge absorption data for KTN, KTaO_3 , and BaTiO_3 are shown in Figs. 3(a), 3(b), and 3(c) as a function of photon energy at several temperatures. These data show an exponential tail of the form

$$\alpha \propto \exp(\beta h\nu). \quad (4)$$

Assuming an Urbach tail²⁶ with $\beta = 1/\eta kT$, where k is Boltzmann's constant and T is the absolute temperature, we find that $\eta \approx 1.67, 1.52, 1.75,$ and 2.50 in $\text{KTaO}_3, \text{BaTiO}_3,$ insulating KTN, and semiconducting KTN, respectively. Data for KTN and BaTiO_3 below the Curie point show that in the ferroelectric phase there are two Urbach absorption edges with $\alpha_{\perp} > \alpha_{||}$. It should be pointed out that our band-edge data for BaTiO_3 are in disagreement with the published data of Casella and Keller.²⁷ Their data, given by the dashed curve in Fig. 3(c), show a much more gradual rise in the absorption coefficient with photon energy than our

²⁵ T. S. Moss, *Optical Properties of Semi-Conductors* (Academic Press Inc., New York, 1961), p. 14. Equation (2) is a simplification which applies here, since $R < 0.2$ over the spectral range of interest.

²⁶ F. Urbach, *Phys. Rev.* **92**, 1324 (1953).

²⁷ R. C. Casella and S. P. Keller, *Phys. Rev.* **116**, 1469 (1959).

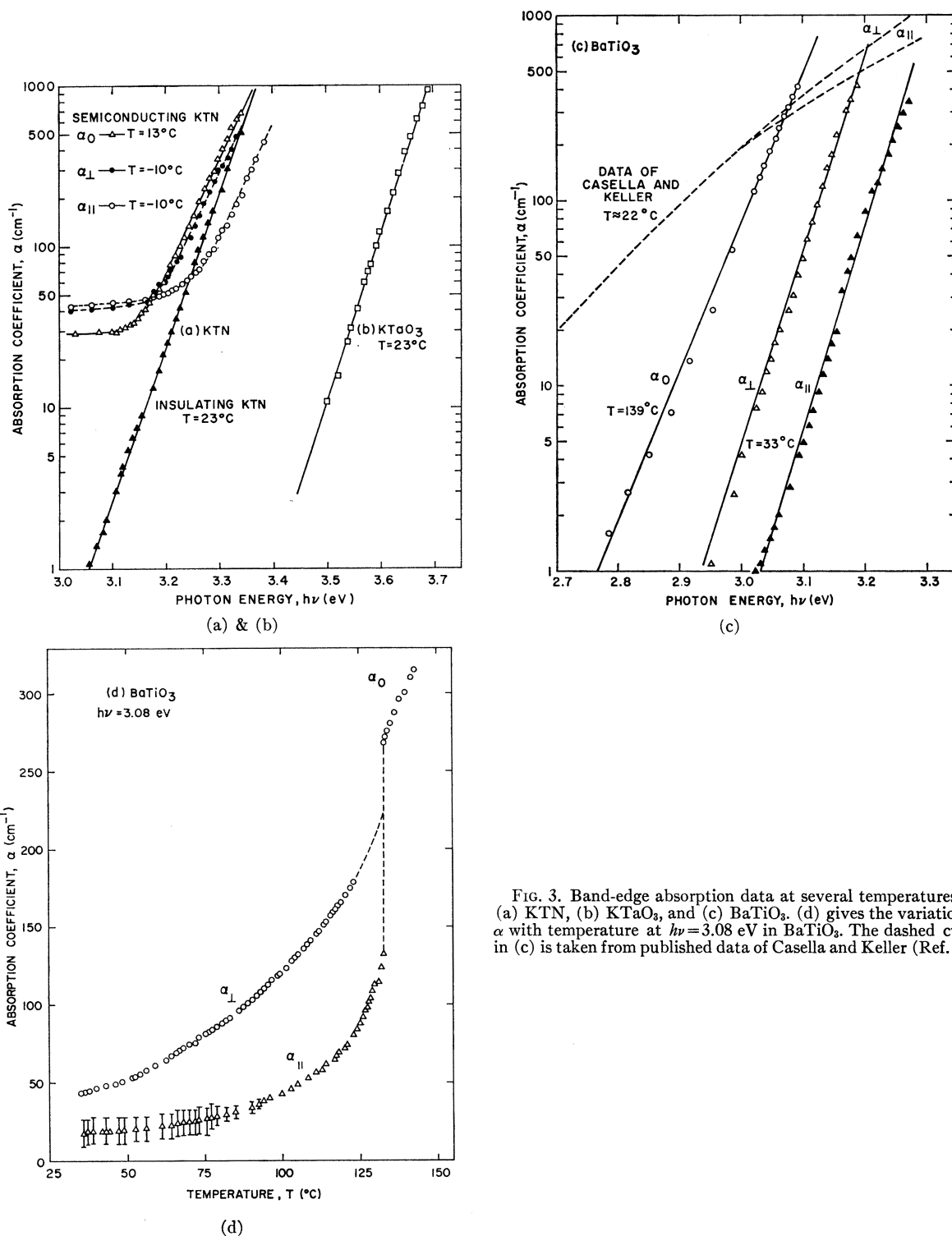


FIG. 3. Band-edge absorption data at several temperatures for (a) KTN, (b) KTaO₃, and (c) BaTiO₃. (d) gives the variation of α with temperature at $h\nu = 3.08 \text{ eV}$ in BaTiO₃. The dashed curve in (c) is taken from published data of Casella and Keller (Ref. 27).

exponential dependence and also show a larger absorption. We believe that the difference may be due to the presence of impurities, possibly fluorine, in their crystals, which were grown by the Remeika method²⁸ from a

²⁸ J. P. Remeika, J. Am. Chem. Soc. **76**, 940 (1954).

KF flux. The data of Fig. 3 were obtained using crystals grown from an excess TiO₂ melt.²⁹ These crystals are almost colorless in large sections. We believe, therefore,

²⁹ A. Linz, V. Belruss, and C. S. Naiman, J. Electrochem. Soc. **112**, 60C (1965).

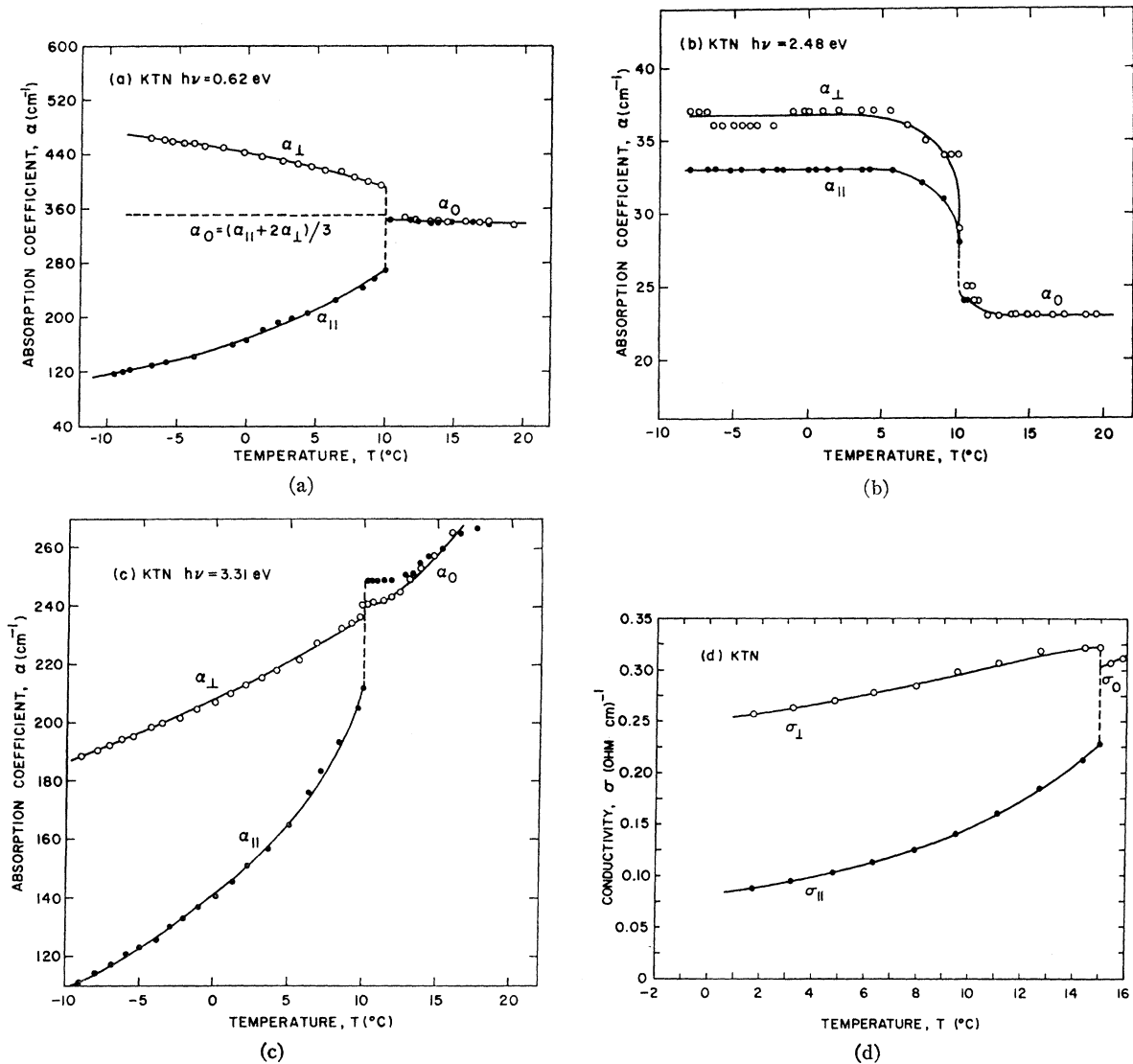


FIG. 4. Temperature dependence of the optical absorption and electrical conductivity in semiconducting KTN having a free-electron concentration of 3×10^{17} cm⁻³. (a) Absorption coefficient α versus temperature T at the peak of the infrared photoionization absorption band $h\nu = 0.62$ eV. The dashed curve for $T < T_c$ is the average absorption $\frac{1}{3}(\alpha_{\parallel} + 2\alpha_{\perp})$. (b) α versus T at $h\nu = 2.48$ eV, (c) α versus T at $h\nu = 3.31$ eV, and (d) electrical conductivity σ versus T on a sample having a Curie temperature of 15°C.

that the band-edge data as well as the dichroism peak reported by Casella and Keller are probably impurity effects. Figure 3(d) shows the temperature dependence of the band-edge absorption in BaTiO₃ at $h\nu = 3.08$ eV. These data, obtained by heating a single-domain insulating crystal, show a first-order phase transition at the Curie point of $T_c = 133$ °C.³⁰

In Fig. 4 we show the temperature dependence of the absorption coefficient in semiconducting KTN at selected photon energies together with the temperature dependence of the dc electrical conductivity. Figure 4(a) gives the variation of α with temperature at the

³⁰ This value for the Curie temperature is thought to be more representative of pure BaTiO₃ than the normally quoted value of 120°C observed in crystals grown from a KF flux (Ref. 28).

peak of the photoionization absorption ($h\nu = 0.62$ eV). At the Curie point $T_c = 10$ °C, an abrupt first-order change in absorption is observed. Below the Curie point α_{\perp} is greater than α_{\parallel} , and both tend to saturate with the spontaneous polarization. Similar data apply throughout the photoionization absorption range, $0.3 < h\nu < 1$ eV. Figure 4(b) gives the variation of α with temperature at $h\nu = 2.48$ eV. In the vicinity of the broad band centered at 0.62 eV, it is observed experimentally that the average absorption $\alpha_0 = (\alpha_{\parallel} + 2\alpha_{\perp})/3$ is independent of the transition. We show in Fig. 4(a) the curve of α_0 derived from the measured values of α_{\parallel} and α_{\perp} in the ferroelectric phase. An outstanding feature of the donor photo-ionization absorption data shown in Fig. 4(a) is the large dichroism developed, $\alpha_{\perp}/\alpha_{\parallel} \approx 4$,

The temperature dependence of the band-edge absorption coefficient at $h\nu=3.31$ eV is shown in Fig. 4(c). These data are representative and apply throughout the band edge. The data given in Fig. 4(c) also show a first-order phase change at $T_c=10^\circ\text{C}$ and once again $\alpha_\perp > \alpha_\parallel$. The band-edge dichroism is also large, attaining the value $\alpha_\perp/\alpha_\parallel \approx 2$. To aid in interpreting the data of Figs. 4(a) and 4(c), we show in Fig. 4(d) the temperature dependence of the dc electrical conductivity measured by a four-terminal method on a KTN sample having a Curie temperature of 15°C . As might be anticipated from the magnitude of the infrared donor photoionization dichroism, the conductivity anisotropy in the ferroelectric phase is large, $\sigma_\perp/\sigma_\parallel \approx 3$. Berglund and Baer¹⁴ report that $\sigma_\perp/\sigma_\parallel \gg 1$ for semiconducting BaTiO₃ as well. A detailed interpretation of the data shown in Figs. 2, 3, and particularly 4 is given in the next section, where the various absorption processes are related to the effects of the spontaneous polarization P_s on the energy-band structure. As we shall show, the energy separation between a -axis and c -axis conduction-band valleys is proportional to P_s^2 , and for this reason we digress at this point to a discussion of optical birefringence data from which we extract the required dependence of P_s on temperature.

B. Birefringence Data

The temperature and wavelength dependence of the birefringence developed in the ferroelectric phase of a semiconducting KTN crystal were measured, using an interference technique. A sample was mounted between

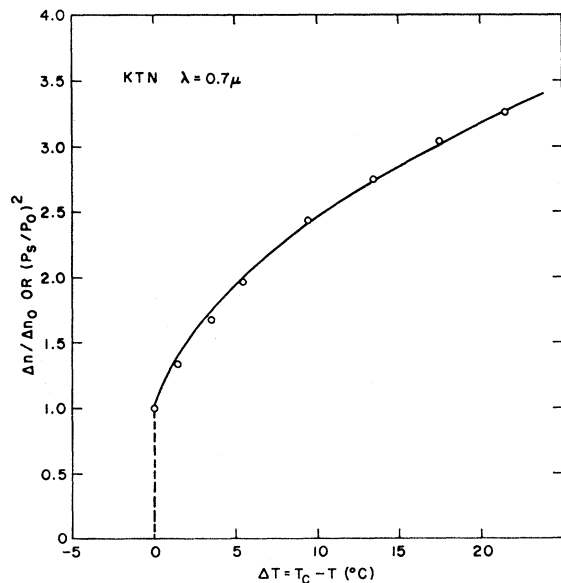


FIG. 5. Temperature dependence of the relative birefringence $\Delta n/\Delta n_0$ at $\lambda=0.7\mu$ (open circles) in semiconducting KTN having 3×10^{17} free electrons. The solid curve is the best fit of $(P_s/P_0)^2$ as a function of $\Delta T = T_c - T$ obtained from Eq. (A8) using $\Delta T_0 = 1.1^\circ\text{C}$.

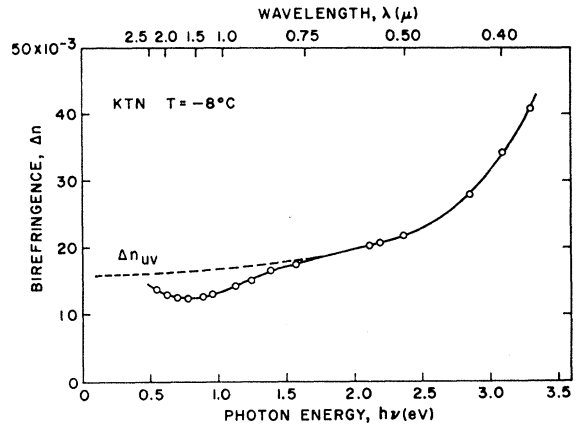


FIG. 6. Spectral dependence of the birefringence Δn for a semiconducting KTN crystal having a free-electron concentration 3×10^{17} cm^{-3} . The solid curve gives Δn versus $h\nu$ at $T = -8^\circ\text{C}$ and the dashed curve gives the extrapolated ultraviolet background birefringence Δn_{UV} calculated from the Sellmeier dispersion relations.

crossed polarizers with the $[001]$ crystal axis at 45° to the polarizer axes; the light was propagated along the $[010]$ axis. The optical transmission through this arrangement was then monitored on a strip chart recorder as a function of sample temperature. The transmission is given by $\sin^2(\Gamma/2)$, where $\Gamma = (2\pi/\lambda)\Delta n l$ is the phase retardation, λ is the wavelength of the light, l is the crystal thickness, and Δn is the crystal birefringence. By using thin crystals, it is possible, at long wavelengths, to ensure that $\Gamma < \pi$ at the ferroelectric transition so that Δn versus T and Δn versus λ can be measured unambiguously from the transmission data.

Figure 5 shows the relative birefringence $\Delta n/\Delta n_0$ (where Δn_0 is the birefringence at the Curie point T_c), measured at $\lambda=0.7\mu$ as a function of temperature for a KTN sample having a carrier concentration of 3×10^{17} cm^{-3} . Similar data apply for $0.35 < \lambda < 2.5\mu$. In a stress-free crystal, the birefringence is related to the quadratic electrooptic coefficients g_{ij} by³¹

$$\Delta n = \frac{1}{2}n^3(g_{11} - g_{12})P_s^2, \quad (5)$$

where P_s is the spontaneous polarization and n is the refractive index in the cubic phase. Equation (5) indicates that at constant wavelength Δn should be related to the temperature dependence of the square of the spontaneous polarization. In the Appendix it is shown in Eq. (A8) how P_s^2 depends on the parameter $\Delta T/\Delta T_0$, where $\Delta T = T_c - T$, $\Delta T_0 = T_c - T_0$, and T_0 is the Curie-Weiss temperature. The solid curve in Fig. 5 is a plot of $(P_s/P_0)^2$ versus T obtained from Eq. (A8) with $\Delta T_0 = 1.1^\circ\text{C}$, the value which gives the best fit to the $\Delta n/\Delta n_0$ experimental data. As can be seen from the curve in Fig. 5, Eq. (5) accurately describes the birefringence in the ferroelectric phase. The parameter P_0 is the lattice

³¹ J. E. Geusic, S. K. Kurtz, L. G. Van Uitert, and S. H. Wemple, Appl. Phys. Letters **4**, 141 (1964).

polarization occurring at the first-order Curie point T_c and is related to the birefringence

$$\Delta n_0 = (n^3/2)(g_{11} - g_{12})P_0^2$$

from Eq. (5). We can make use of this relation to determine P_0 by taking $g_{11} - g_{12}$ and n to have the same values as in insulating KTN.^{31,32} At $\lambda = 0.7 \mu$, $\Delta n_0 = 6.0 \times 10^{-3}$, $g_{11} - g_{12} = 0.14 \text{ m}^2/\text{C}^2$, and $n = 2.27$, giving $P_0 = 0.086 \text{ C/m}^2$ in substantial agreement with existing published data.³²

As shown in Fig. 6, in the range of photon energies between 0.5 and 1.5 eV there is a small *negative* contribution to the birefringence given by $\Delta n_{ir} = \Delta n - \Delta n_{uv}$, where Δn_{uv} is the background birefringence produced by optical absorption in the ultraviolet. This excess negative birefringence Δn_{ir} can be shown to be related to the infrared-absorption dichroism through the Kramers-Kronig relations.

4. INTERPRETATION OF THE ABSORPTION DATA

A. Absorption Edge

The absorption data presented in the preceding section can be interpreted in terms of the many-valley KL tight-binding band scheme, which applies in the paraelectric phase, and Brews's modified band scheme, which applies in the ferroelectric phase. Both band schemes are given over a limited portion of the Brillouin zone in Fig. 1. In view of the uncertainties in the valence-band structure and the low-energy exponential tailing off the interband absorption edge, it is difficult to make a definite assignment to the fundamental interband transition. We note, however, that Baer¹⁷ has shown from Faraday rotation measurements that these transitions are probably direct. They can concur, therefore, at either the zone center (Γ point) or zone boundary (X point). By considering the effect of the lattice polarization on the various critical points as calculated by Brews, we shall show that the temperature dependence of the band-edge dichroism can be interpreted consistently with other data, such as electrical conductivity, in terms of direct transitions occurring at the X point, i.e., $X_{5'} \rightarrow X_3$ ($X_{4'} \rightarrow X_3$ is forbidden). Referring to Fig. 1(a) we note that it is possible for the indirect $\Gamma_{15} \rightarrow X_3$ transition to occur at lower energy than the direct zone boundary $X_{5'} \rightarrow X_3$ transition. We believe that the Urbach tail observed experimentally is due to multiphonon-assisted $X_{5'} \rightarrow X_3$ transitions as discussed recently by Mahan³³ and that this masks the weaker $\Gamma_{15} \rightarrow X_3$ indirect transition. Adopting this as the fundamental interband transition, we can compute the absorption anisotropy per valley in both paraelectric and ferroelectric phases and then sum over the three valleys to obtain the absorption coefficient. This model

attributes the entire absorption anisotropy for $T < T_c$ to an energy splitting between a -axis (X_{\perp}) and c -axis (X_{\parallel}) conduction-band valleys [see Fig. 1(b)]. Our interpretation differs from that recently given by Casella,¹⁶ who attributes the absorption anisotropy to valence-band splittings and associated selection rules.

To compute the relative magnitudes of the absorption coefficients for light polarized along the a and c axes it is convenient to define oscillator strengths f_{vc}^a and f_{vc}^c per valley. The subscript vc denotes valence-to conduction-band transitions, and the superscripts l and t denote, respectively, longitudinal and transverse mass directions. By using the KL symmetrized wave functions, the selection rules $f_{vc}^a \neq 0$ and $f_{vc}^c \approx 0$ are obtained. Since the band-edge absorption coefficient has an exponential Urbach tail, we may define interband absorption coefficients per valley as

$$a_l = \gamma f_{vc}^l \exp[\beta(h\nu - \varepsilon)], \quad (6a)$$

$$a_t = \gamma f_{vc}^t \exp[\beta(h\nu - \varepsilon)], \quad (6b)$$

where γ is a constant of proportionality which includes the joint density of states, ε is the band-gap energy, and $\beta = 1/\eta kT$ as defined in Eq. (4). In the paraelectric phase there are three equivalent valleys giving a total isotropic absorption coefficient ($\alpha_0 = 2a_t + a_l$)

$$\alpha_0 = 2\gamma f_{vc}^t \exp[\beta(h\nu - \varepsilon_0)], \quad (7)$$

where we have taken $f_{vc}^l \approx 0$. In the ferroelectric phase defining the c -axis and a -axis valley energies as ε_c and ε_a , respectively, and using $f_{vc}^c \approx 0$, we obtain for the anisotropic absorption coefficients

$$\alpha_{\parallel} = 2\gamma f_{vc}^t \exp[\beta(h\nu - \varepsilon_a)], \quad (8a)$$

$$\alpha_{\perp} = \gamma f_{vc}^t \{ \exp[\beta(h\nu - \varepsilon_c)] + \exp[\beta(h\nu - \varepsilon_a)] \}. \quad (8b)$$

In this analysis we assume that the oscillator strengths are insensitive to the lattice polarization, i.e., polarization-induced changes in the valley shapes are negligible. It is convenient to normalize α_{\parallel} and α_{\perp} with respect to α_0 and define $\Delta\varepsilon = \varepsilon_a - \varepsilon_c$, giving

$$\alpha_{\parallel}/\alpha_0 = \exp[\beta(\varepsilon_0 - \varepsilon_a)] \quad (9a)$$

and

$$\alpha_{\perp}/\alpha_0 = \frac{1}{2}[1 + \exp(\beta\Delta\varepsilon)] \exp[\beta(\varepsilon_0 - \varepsilon_a)]. \quad (9b)$$

Using this model we can determine the temperature dependence of $\beta\Delta\varepsilon$ and $\beta(\varepsilon_0 - \varepsilon_a)$ from the experimentally determined values of α_{\perp}/α_0 and $\alpha_{\parallel}/\alpha_0$. Because the crystals are centrosymmetric above T_c , we expect $\beta\Delta\varepsilon \propto P_s^2$ below T_c . To check this possibility we have plotted $\beta\Delta\varepsilon$ as a function of $(P_s/P_0)^2$ in Fig. 7 for both KTN and BaTiO₃ by using Eq. (A8) and the parameter $\Delta T_0 = 1.1^\circ\text{C}$ previously determined from birefringence measurements for KTN and $\Delta T_0 = 11 - 16^\circ\text{C}$ for BaTiO₃.³⁴ A nearly linear relationship is

³² F. S. Chen, J. E. Geusic, S. K. Kurtz, J. G. Skinner, and S. H. Wemple, *J. Appl. Phys.* **37**, 388 (1966).

³³ G. D. Mahan, *Phys. Rev.* **145**, 602 (1966).

³⁴ The value $\Delta T_0 \approx 11^\circ\text{C}$ is taken from data of W. J. Merz, *Phys. Rev.* **91**, 513 (1953). Data of M. E. Drougard, R. Landauer, and D. R. Young, *Phys. Rev.* **98**, 1010 (1955) give $\Delta T_0 \approx 14^\circ\text{C}$. Recent data of C. J. Johnson, *Appl. Phys. Letters* **7**, 221 (1965) give $\Delta T_0 \approx 16^\circ\text{C}$ for crystals similar to those used in the present study.

found with

$$\beta\Delta\epsilon_{\text{KTN}} \approx 0.28(P_s/P_0)^2 \text{ for KTN} \quad (10a)$$

and

$$\beta\Delta\epsilon_{\text{BaTiO}_3} \approx 0.90(P_s/P_0)^2 \text{ for BaTiO}_3. \quad (10b)$$

For KTN, using $P_0 = 0.086 \text{ C/m}^2$ obtained from birefringence data and $\beta = 1/\eta kT$ with $\eta = 2.50$ [see Fig. 3(a)], we obtain

$$\Delta\epsilon_{\text{KTN}} \approx 2.2P_s^2 \text{ eV}, \quad (11)$$

where P_s is in C/m^2 . Similarly for BaTiO_3 using $P_0 = 0.18 \text{ C/m}^2$ (see Table I) and $\eta = 1.52$ [see Fig. 3(c)] we obtain³⁵

$$\Delta\epsilon_{\text{BaTiO}_3} \approx 1.5P_s^2 \text{ eV}. \quad (12)$$

Frova³⁶ has observed a similar shift of the conduction-band edge in KTaO_3 , using electroabsorption data. His value, $\Delta\epsilon_{\text{KTaO}_3} \approx 2.0P_s^2 \text{ eV}$, compares favorably with our results. We note that both Frova's data and ours are in good agreement with the predictions of Brews.¹⁵ We also note that our result for BaTiO_3 is in excellent agreement with the band-edge energy shift obtained by Gähwiler³⁷ at 25°C from electroreflectance measurements.

From the band-edge data shown in Fig. 3, values for

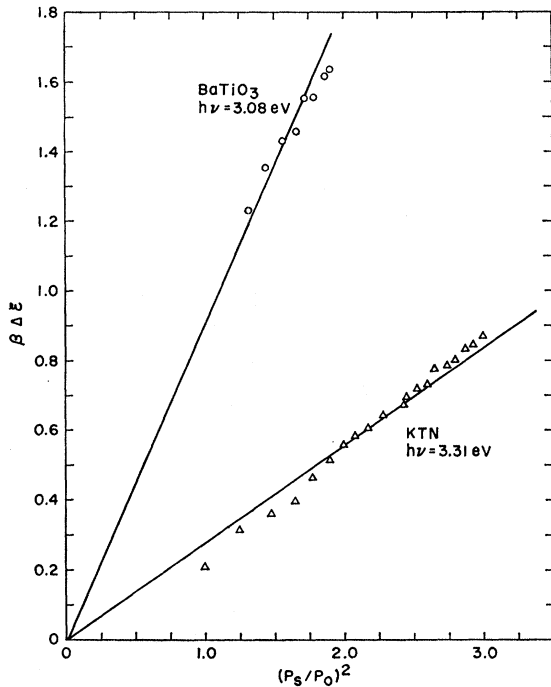


FIG. 7. $\beta\Delta\epsilon$ as a function of $(P_s/P_0)^2$ for KTN and BaTiO_3 . $\Delta\epsilon$ is the energy shift between valleys perpendicular to and parallel to the direction of P_s .

³⁵ Since ΔT_0 is known only imprecisely and may fall between 11 and 16°C , a corresponding uncertainty exists in the coefficient of $(P_s/P_0)^2$ in Eq. (10b), giving rise to a range of values in Eq. (12) of 1.5 ± 0.2 .

³⁶ A. Frova, Nuovo Cimento (to be published).

³⁷ Ch. Gähwiler, Solid State Commun. **5**, 65 (1967).

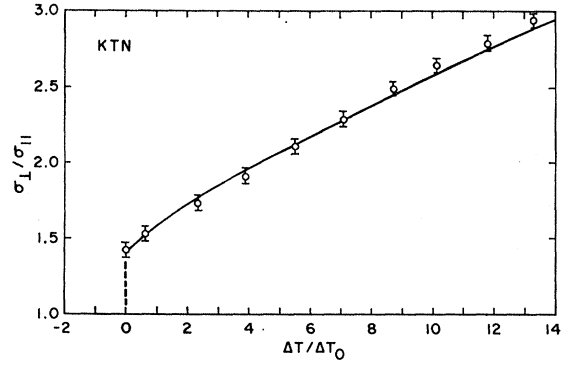


FIG. 8. Temperature dependence of the electrical-conductivity anisotropy in semiconducting KTN having a free-electron concentration of $3 \times 10^{17} \text{ cm}^{-3}$. The curve is computed from Eq. (13) using values of $\Delta\epsilon$ computed from Eq. (11) and $K = 10$; the open-circle data points are obtained from Fig. 4(d).

the direct band gap at the X point can be estimated. To do this we make use of Mahan's interpretation of an Urbach interband edge.³³ Mahan suggests that such an exponential tail is an intrinsic property of certain polar materials in which an electron-optical-phonon (polaron) interaction involving several phonons gives an approximately exponential tail to the spectral density function. According to this theory we expect the band gap to be a few high-energy longitudinal optical (LO) phonons above the energy where the absorption coefficient α stops increasing exponentially. For all the perovskites shown in Fig. 3, α is still increasing exponentially at $\alpha \approx 10^3 \text{ cm}^{-1}$. From ultraviolet reflectivity data² we estimate that α reaches $\approx 10^4 \text{ cm}^{-1}$ at $h\nu \approx 4 \text{ eV}$. Thus, the absorption coefficient increases much less rapidly with photon energy in the range $\alpha \approx 10^3 - 10^4 \text{ cm}^{-1}$ than in the exponential tail ($\alpha \lesssim 10^3 \text{ cm}^{-1}$). Based on Mahan's treatment we expect the true band gap to fall one or two LO phonons above the $\alpha \approx 10^3 \text{ cm}^{-1}$ absorption point giving rise to the estimated band gaps listed in Table I. These values are close to those calculated by Baer¹⁷ from interband Faraday rotation data.

Having obtained values for the conduction-band valley shifts as a function of spontaneous polarization in KTN, it is of interest to determine whether these shifts are quantitatively consistent with electrical-conductivity anisotropy data in semiconducting crystals. We assume a model in which the deep donor levels ($\approx 0.3 \text{ eV}$) remain fixed with respect to the valence band when the crystal transforms from the cubic to tetragonal state. As a result of the transformation, the energy difference $\Delta\epsilon$ induced between a -axis and c -axis valleys by the lattice polarization causes electrons to repopulate between these valleys. It can then be shown, for deep donors, that the conductivity ratio $\sigma_{\perp}/\sigma_{\parallel}$ is given by

$$\frac{\sigma_{\perp}}{\sigma_{\parallel}} = \frac{K + (1+K) \exp(-\Delta\epsilon/kT)}{1 + 2K \exp(-\Delta\epsilon/kT)}, \quad (13)$$

where $K = \mu_t/\mu_l$ is a mobility anisotropy coefficient be-

tween transverse (μ_t) and longitudinal (μ_l) valley mobilities. Since the temperature dependence of $\Delta\mathcal{E}$ is known, K can be found by fitting Eq. (13) to the conductivity anisotropy data shown in Fig. 4(d). This is done in Fig. 8, where $\sigma_{\perp}/\sigma_{\parallel}$ is plotted versus the reduced temperature $\Delta T/\Delta T_0$, using the energy splitting $\Delta\mathcal{E}$ given by Eq. (11), $\Delta T_0 = 1.1^\circ\text{C}$, and $K = 10$. As can be seen, the fit is quite good over the full temperature range. We point out that the anisotropy constant $K = 10$ is unexpectedly large. From the definition of K we have

$$K = (m_t^*/m_l^*)(\tau_t/\tau_l), \quad (14)$$

in which τ_t and τ_l are, respectively, transverse and longitudinal relaxation times. Magnetoresistance measurements^{7,13} on SrTiO₃ and KTaO₃ at 4.2°K give $K \approx 4$. Our room-temperature value of $K = 10$ can then be interpreted in terms of a collision-time ratio (τ_t/τ_l), approximately 2.5 times greater than the low-temperature ratio, if we assume a temperature-independent mass.

B. Donor Photo-Ionization

The broad infrared absorption band shown in Fig. 2(a) is due to photoionization of filled deep donors. To test this conclusion, relative absorption data were taken at 77°K, where nearly all electrons are known to freeze out on the donors, thereby eliminating any possibility of a free-carrier contribution. These data show no significant temperature dependence in the vicinity of the 0.62-eV absorption peak. At lower energies, however, an absorption threshold is observed near 0.35 eV in substantial agreement with the donor ionization energy deduced from Hall-effect measurements.

The spectral dependence of photo-ionization absorption due to deep-lying donors in semiconductors has been considered by Lucovsky.³⁸ He considers a simple model in which the conduction band is parabolic, and the donor can be described in terms of a short-range ion-core potential rather than the long-range Coulomb potential appropriate for shallow donors. In a zero-range or δ -function approximation, the donor wave function is s like, and use of time-dependent perturbation theory gives $\alpha \propto (h\nu - \mathcal{E}_D)^{3/2}/(h\nu)^3$, where \mathcal{E}_D is the donor binding energy. This model predicts that the donor photoionization absorption will reach a maximum at $h\nu = 2\mathcal{E}_D$ and fall off as $(h\nu)^{-3/2}$ for $h\nu \gg \mathcal{E}_D$. In contrast, for hydrogenic donors, the absorption has a maximum at $h\nu = \mathcal{E}_D$ and falls off as $(h\nu)^{-3}$ for $h\nu \gg \mathcal{E}_D$. It should be noted that the rate at which the photo-ionization absorption falls off with photon energy as well as the precise position of the peak absorption depends on the nature of both the band structure and the impurity-center ion-core potential. The parabolic band approximation may be in considerable error in the perovskite oxides particularly when $h\nu > 1$ eV. This is expected to cause deviations from the $(h\nu)^{-3/2}$ falloff predicted by

Lucovsky. Experimentally, the data for KTN show $\alpha \propto (h\nu)^{-3.8}$. For photon energies falling between the threshold and the peak ($0.35 \lesssim h\nu \lesssim 0.62$ eV), effects of nonparabolicity and contributions from other bands are reduced so that the observed peak at 0.62 eV does indeed fall at approximately twice the donor ionization energy. Accordingly, we shall assume the donor wave functions to be highly localized s states determined by the δ -function core-potential approximation used by Lucovsky.

In our analysis of the photo-ionization-absorption data (as with the conductivity data analysis) we assume that the donor level remains fixed with respect to the valence band both above and below the Curie point, and that this level is spread throughout almost the entire Brillouin zone because of the physical localization of the donor electron to approximately one unit cell. Following the analysis of the interband-absorption data given above, the photo-ionization absorption can be analyzed similarly in terms of oscillator strengths *per valley* from the donor level to the $\Delta_{2'}$, Z_4 , and Δ_5 conduction-band levels. The applicable selection rule is the same as in the interband case, i.e., the longitudinal oscillator strengths are expected to be negligible compared to the transverse oscillator strengths. In KTN at low photon energies, $h\nu \lesssim 1$ eV, transitions to $\Delta_{2'}$ and Z_4 are expected to dominate due to the non-negligible downward bending of the $\Delta_{2'}$ level between $\Gamma_{25'}$ and X_3 by about 0.3–0.4 eV (see Table I). This leads, in the vicinity of the conduction-band minimum, to a single transverse oscillator strength. At higher photon energies, $h\nu \gtrsim 1$ eV, transitions to Δ_5 must be included. Referring to the data shown in Fig. 2(a), we attribute the decrease in absorption for $h\nu > 0.62$ eV to a decrease in oscillator strength as electrons are photoexcited toward the Z_2 level. From ultraviolet reflectivity data, Kurtz² has estimated that in KTN Z_2 at the X_3 point lies approximately 2 eV above Z_4 at the X_3 point, giving an energy separation of about 2.3 eV between the donor level and Z_2 . The energy-band calculations of Brews¹⁵ and Zook and Casselman³⁹ predict an upward shift of the flat Z_2 conduction-band level along the c axis in the ferroelectric phase relative to its position in the paraelectric phase. This is consistent with the data given in Fig. 4(b), which show that in the visible where $h\nu$ is sufficiently large to excite electrons to the vicinity of Z_2 the absorption coefficient increases at the ferroelectric transition for both polarizations.

Considering transitions to the vicinity of the conduction-band minima we have for $h\nu \lesssim 1$ eV one transverse oscillator strength f_0' in the paraelectric phase. The absorption coefficient per valley is $a = \kappa f_0'^2 N_D$, where κ is a constant of proportionality which includes the density of final states, and N_D are the number of occupied donors. Summing over the three valleys with

³⁸ G. Lucovsky, Solid State Commun. **3**, 299 (1965).

³⁹ J. D. Zook and T. N. Casselman, Phys. Rev. Letters **17**, 960 (1966).

polarized light gives

$$\alpha_0 = 2\kappa f_0^t N_D. \quad (15)$$

In the ferroelectric phase we have oscillator strengths f_c^t and f_a^t for the c -axis and a -axis valleys, respectively. We neglect here as before any distortions in the shape of the energy surfaces and assume that the only effect of the ferroelectric transition is to shift levels relative to one another. With polarized light we obtain

$$\alpha_{||} = 2\kappa f_a^t N_D, \quad (16a)$$

$$\alpha_{\perp} = \kappa (f_c^t + f_a^t) N_D. \quad (16b)$$

It is important to recognize that the oscillator strengths are functions of frequency through their dependence on the matrix elements between the fixed donor ground state and the conduction-band states. For purposes of further analysis it is useful to consider the ratios

$$\alpha_{||}/\alpha_0 = f_a^t/f_0^t, \quad (17a)$$

$$\alpha_{\perp}/\alpha_0 = (f_c^t + f_a^t)/2f_0^t. \quad (17b)$$

By combining these equations with the experimentally determined relation $2\alpha_{\perp} + \alpha_{||} = 3\alpha_0$ [see Fig. 4(a)], we obtain an experimental oscillator strength sum rule given by

$$f_0^t = \frac{1}{3} (f_c^t + 2f_a^t). \quad (18)$$

This f sum rule describes an important conservation principle for the allowed transitions above and below the Curie point among the three conduction-band valleys. Equation (18) indicates that in the ferroelectric phase f_c^t and f_a^t must change with temperature in such a way that their weighted average remains constant.

These results lead to the following observations: Since $\alpha_{||}/\alpha_0 < 1$, Eq. (17a) demands that

$$f_a^t/f_0^t < 1, \quad (19a)$$

in which case, from Eq. (18),

$$f_c^t/f_0^t = 3 - 2f_a^t/f_0^t > 1. \quad (19b)$$

From Eqs. (17) and (19) we note that whereas $\alpha_{||}/\alpha_0$ varies directly as f_a^t/f_0^t , α_{\perp}/α_0 varies as $\frac{1}{2}(3 - f_a^t/f_0^t)$ and consequently should approach $\frac{3}{2}$ as f_a^t/f_0^t decreases. The data given in Figs. 2(a) and 4(a) are consistent with this prediction. Furthermore, since the a -axis valleys shift to higher energies according to Eq. (11), viz., $\Delta\epsilon \propto P_s^2$, we expect that the threshold energy where f_a^t begins increasing rapidly should shift to higher energies relative to the threshold for f_0^t by approximately $\Delta\epsilon$. From Eq. (17a) the peak in $\alpha_{||}$ should therefore shift to higher energies proportional to P_s^2 . On the other hand, since the c -axis valleys are relatively stationary, f_c^t is expected to remain nearly constant, as indicated by Eq. (19b). We therefore expect from

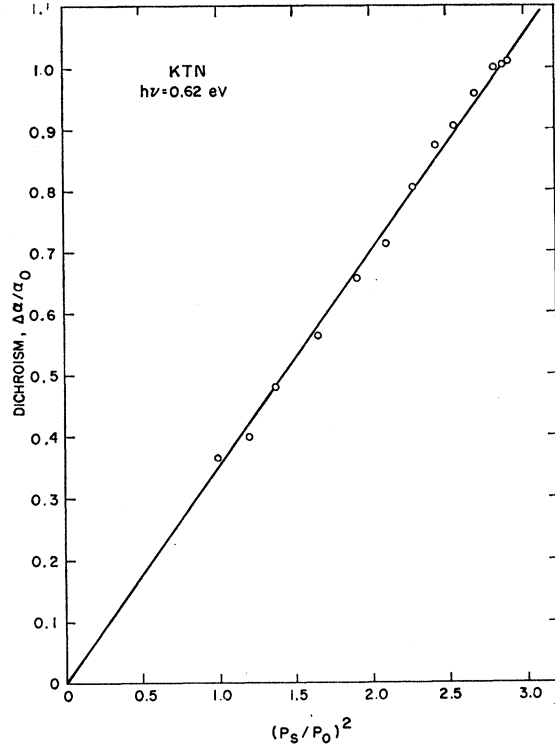


FIG. 9. Dichroism $\Delta\alpha/\alpha_0$ at the infrared-absorption peak of $h\nu=0.62$ eV in semiconducting KTN versus $(P_s/P_0)^2$.

Eq. (17b) that the peak of α_{\perp} should be nearly independent of temperature. These conclusions are borne out by the observed shifts of the photo-ionization-absorption peaks which show the peak of $\alpha_{||}$ shifting toward higher energies by approximately 35 meV for $(P_s/P_0)^2 \approx 3$ and the peak of α_{\perp} remaining nearly constant. The magnitude and the polarization dependence of the shift is consistent with Eq. (11) to within the rather large error limits (± 10 meV) inherent in the determination of the peak of a broad absorption band.

Shown in Fig. 9 is a plot of the experimental $\Delta\alpha/\alpha_0$ data at $h\nu=0.62$ eV versus $(P_s/P_0)^2$. The dichroism is observed to depend quadratically on the spontaneous polarization for values of $\Delta\alpha/\alpha_0$ as large as one [$\Delta\alpha/\alpha_0 = 0.35(P_s/P_0)^2$]. An expression for the dichroism ($\Delta\alpha/\alpha_0$) can be obtained in terms of f_a^t/f_0^t from Eqs. (17) and (19b) with the result

$$\Delta\alpha/\alpha_0 = \frac{3}{2}(1 - f_a^t/f_0^t). \quad (20)$$

This result combined with the data of Fig. 9 imply a quadratic dependence of $f_0^t - f_a^t$ on spontaneous polarization.

5. CONCLUSIONS

Several conclusions may now be drawn regarding the electron energy-band structure of the perovskite oxides. The most important is that the KL many-valley energy-band scheme together with the lattice-polarization-

dependent modifications calculated by Brews¹⁵ are consistent with the band-edge absorption data, the shifts in the peaks of the α_{11} and α_{11} photo-ionization curves, and the electrical-conductivity anisotropy measurements. We interpret, on the basis of this energy-band model and Baer's Faraday rotation data,¹⁷ that the interband transition threshold is probably direct at the zone boundary between $X_{5'}$ and X_3 . Kurtz² has attributed the lowest energy-absorption threshold seen in ultraviolet reflectivity to this same transition. The band-edge data shown in Fig. 3 are masked by a low-energy exponential tail which we interpret as an intrinsic phonon interaction based on Mahan's³³ theoretical calculations and the fact that all of the perovskite oxides studied (see Table I) exhibit this property. We should emphasize that the band-edge data for BaTiO₃ shown in Fig. 3(c) are new and in disagreement with the published results of Casella and Keller.²⁷ Our data analysis has also enabled us to show that the effect of the spontaneous polarization P_s is largely to shift the energy of the a -axis valleys upward by an amount $\Delta\epsilon = 2.2P_s^2$ eV for KTN and $\Delta\epsilon = 1.5P_s^2$ eV for BaTiO₃, where P_s is in C/m².

A second conclusion which may be drawn is that the donor photo-ionization data can be understood in terms of transitions from filled donor levels to the Z_4 and Δ_5 conduction-band states. In KTN, where the donors are deep and as a consequence are thought to have a $1s$ -state configuration, transitions to the level Z_4 (determining the transverse effective mass) dominate, since the $\Delta_{2'}$ bending is relatively large (≈ 0.3 eV). In this case the photoionization absorption is observed to obey a simple f sum rule for transitions among the three conduction-band valleys [see Eq. (18)]. The average absorption is found to be independent of temperature and unaffected by the ferroelectric transition. The dichroism at the infrared-absorption peak is observed to vary quadratically with spontaneous polarization according to $\Delta\alpha/\alpha_0 = 47P_s^2$, where P_s is in C/m². We may speculate that in BaTiO₃, where the bending of the $\Delta_{2'}$ level is relatively small (≈ 0.1 eV), transitions to Δ_5 , occurring in the longitudinal mass direction, will become as important as those to Z_4 . In this case we expect reduced donor photo-ionization dichroism and a breakdown of the sum rule.

ACKNOWLEDGMENTS

We wish to thank E. F. Kankowski and I. Camlibel for their assistance in performing the experimental work. We are grateful to W. A. Bonner and L. G. Van Uitert

for the KTN crystals and to A. Linz of MIT for the BaTiO₃ crystals. Finally, we acknowledge having several informative discussions with S. K. Kurtz and J. R. Brews.

APPENDIX

Thermodynamic Derivation of P_s versus T

For centrosymmetric crystals in which the crystal polarization P is along one of the crystallographic axes, the free energy in the zero stress limit can be written in one dimension as

$$F = \frac{1}{2}\chi P^2 + \frac{1}{4}\xi P^4 + \frac{1}{6}\zeta P^6 + \dots, \quad (\text{A1})$$

where χ , ξ , and ζ are constants dependent on temperature. The coefficient χ is related to the low-field dielectric constant ϵ in the paraelectric phase. For large ϵ , $\chi = 1/\epsilon$, whereupon

$$\chi = (T - T_0)/\epsilon_0 C. \quad (\text{A2})$$

Here T_0 is the Curie-Weiss temperature, C is the Curie constant, and ϵ_0 is the permittivity of free space. At the transition temperature T_c , by combining the equation $F = 0$ and $E = \partial F/\partial P = 0$ (E is the electric field), we obtain the relation

$$P_0^2 = -\frac{3}{4}(\xi/\zeta), \quad (\text{A3})$$

where for first-order transitions $\xi < 0$. Below the transition temperature ($T < T_c$), $E = \partial F/\partial P = 0$, so that the spontaneous polarization P_s must satisfy

$$\chi + \xi P_s^2 + \zeta P_s^4 = 0. \quad (\text{A4})$$

By defining $\Delta T = T_c - T$ and $\Delta T_0 = T_c - T_0$, we can rewrite Eq. (A2) as

$$\epsilon_0 C \chi = \Delta T_0 - \Delta T. \quad (\text{A5})$$

Substituting Eqs. (A3) and (A5) into (A4) with $\Delta T = 0$ gives

$$\Delta T_0 = (3/16)(\xi^2/\zeta)\epsilon_0 C. \quad (\text{A6})$$

Below the ferroelectric phase transition we therefore obtain from Eq. (A4) together with Eqs. (A3), (A5), and (A6) the following quadratic relation for the spontaneous polarization P_s in terms of ΔT :

$$3(P_s/P_0)^4 - 4(P_s/P_0)^2 + (1 - \Delta T/\Delta T_0) = 0. \quad (\text{A7})$$

Solving for $(P_s/P_0)^2$ we obtain

$$(P_s/P_0)^2 = \frac{2}{3}\{1 + \frac{1}{2}[1 + 3(\Delta T/\Delta T_0)]^{1/2}\}. \quad (\text{A8})$$